Molecular Dynamics Simulation of Shear- and Stretch-Induced Dissociation of P-Selectin/PSGL-1 Complex

Yingyong Kang,[△] Shouqin Lü,[△] Peng Ren, Bo Huo,* and Mian Long*
Key Laboratory of Microgravity (National Microgravity Laboratory) and Center for Biomechanics and Bioengineering, Institute of Mechanics, Chinese Academy of Sciences, Beijing, People's Republic of China

ABSTRACT By mediating the tethering and rolling of leukocytes on vascular surfaces, the interactions between P-selectin and the P-selectin glycoprotein ligand 1 (PSGL-1) play crucial roles during inflammation cascade. Tensile stretch produced by rolling leukocytes and shear stress exerted by blood flow constitute the two types of mechanical forces that act on the P-selectin/PSGL-1 bond. These forces modulate not only dissociation kinetics of this bond, but also the leukocyte adhesion dynamics. However, the respective contribution of the two forces to bond dissociation and to the corresponding microstructural bases remains unclear. To mimic the mechanical microenvironment, we developed two molecular dynamics approaches; namely, an approach involving the shear flow field with a controlled velocity gradient, and the track dragging approach with a defined trajectory. With each approach or with both combined, we investigate the microstructural evolution and dissociation kinetics of the P-LE/SGP-3 construct, which is the smallest functional unit of the P-selectin/PSGL-1 complex. The results demonstrate that both shear flow and tensile stretch play important roles in the collapse of the construct and that, before bond dissociation, the former causes more destruction of domains within the construct than the latter. Dissociation of the P-LE/SGP-3 construct features intramolecular destruction of the epidermal-growth-factor (EGF) domain and the breaking of hydrogen-bond clusters at the P-selectin-lectin/EGF interface. Thus, to better understand how mechanics impacts the dissociation kinetics of the P-selectin/PSGL-1 complex, we propose herein two approaches to mimic its physiological mechanical environment.

INTRODUCTION

P-selectin is a member of the selectin family and is expressed on activated endothelium and platelets (1). One of its ligands, P-selectin glycoprotein ligand-1 (PSGL-1), is constitutively expressed on leukocytes (2). Interactions between P-selectin and PSGL-1 play crucial roles in mediating the tethering and rolling of leukocytes on postcapillary venular surfaces during the initial stage of inflammation cascade, which is a necessary stage for leukocytes to further adhere to the surface before finally penetrating through the venule into the inflamed tissues (3,4). To support smooth rolling of leukocytes, the dissociation of a P-selectin/PSGL-1 bond in the rear of the cell should be balanced with the formation of another bond at the front. During this process, two types of mechanical forces act on the complexes, which further regulate the dissociation kinetics for the dynamic balance of leukocytes (5,6). These two mechanical forces are tensile stretch, which is induced by the rolling of the leukocytes, and shear stress, which is exerted by blood flow near the venular surface. Here, tensile stretch is exerted via cell rolling at one end of the complex and extends along the principal axis of the complex, whereas shear flow acts on the entire molecule with a velocity gradient perpendicular to the venular surface (7).

In previous work, the researchers experimentally investigated the effects of tensile stretch on P-selectin/PSGL-1 bond dissociation using techniques such as atomic force microscopy, biomembrane force probe, and optical tweezers (5,8–10). Furthermore, they used steered molecular dynamics simulation (SMD) to elucidate the microstructural bases of P-selectin unfolding (11) and P-selectin/PSGL-1 bond dissociation under mechanical stretch (12) and proposed a sliding-rebinding model to explain the catch bond at atomic level (13). However, along the preset direction the uniaxial stretch with constant force or constant velocity in these measurements and simulations is distinct from the physiological case where the mechanical stretch is applied in a time-varying direction and magnitude determined by the rolling leukocyte. Thus, a new approach is desirable to manipulate the movement of this molecular complex under a physiologically relevant stretch.

The flow-chamber technique is ideal for measuring the kinetic features of the P-selectin/PSGL-1 complex at the cell level when both tensile stretch and shear stress are exerted (5,14,15). But it is difficult to isolate the impact of shear flow from that of tensile stretch. Molecular dynamics (MD) simulation might be a useful tool to study the effect of shear flow on the microstructural evolution of the complex. Previously, a flow field with constant velocity was established to study the flow-induced structural transition of glycoprotein Ib, in which a constant force was applied to each atom in a layer upstream of the interested molecule (16–18). The uniform flow field described in these studies may be applicable for the short 16-residue peptide, but a flow field with a nonzero velocity gradient should be more reasonable for the P-selectin/PSGL-1 complex, which is >1000-residues long.

Submitted July 17, 2011, and accepted for publication November 21, 2011.

[△]Yingyong Kang and Shouqin Lü contributed equally to this work.

*Correspondence: mlong@imech.ac.cn or huobo@imech.ac.cn

Editor: Nathan Baker.

0006-3495/12/01/0112/9 $2.00

doi: 10.1016/j.bpj.2011.11.4002

Only a few works have reported the flow field construction with a preset velocity gradient. For example, researchers created a Poiseuille flow by applying an external force on each solvent particle within the entire field (19), and a Couette flow was created by moving the upper plane to drag the below-solvent particles (20). However, the former produces compulsive flow by enforcing each solvent particle to move, which should not be the case in reality, especially for those solvent particles very close to the macromolecule. The latter takes a very long time to generate a flow field with various velocities due to the low efficiency of the momentum delivery from the mobile plane to the neighboring molecules, which would be time-consuming when performing macromolecule simulations under flow. Therefore, a fully developed shear flow with a preset linear velocity distribution is required to mimic physiological blood flow.

In this study, we use MD simulation to develop two ways to address the problem: the shear flow field (SFF) with constant velocity gradient and the track-dragging approach (TDA) with a defined trajectory. Using these methods, we elucidate herein the impact of shear flow and/or tensile stretch on the dissociation dynamics of the P-LE/SGP-3 construct, which is an effective binding unit of the P-selectin/PSGL-1 complex (21). Microstructural bases of bond dissociation are then analyzed under mechanical conditions that mimic the physiological situation.

MATERIALS AND METHODS

System construction and equilibration

Two systems were constructed: a cubic water system (CWS) consisting of only water molecules to evaluate the shear-flow simulation method, and a molecular complex system (MCS) to evaluate the impacts of shear flow and/or tensile stretch. The MCS system was built by solvating P-LE/SGP-3 (Protein DataBank code: 1G1S) into a water box and neutralizing it with ~100 mM Na^+ and Cl^- ions. The water molecules and the ions were created using SOLVATE1.2 and AUTOIONIZE1.3 plugins for VMD (22). The force-field parameters of CHARMM22 were adopted to describe water molecules (23), peptides, and ions (24,25) in P-LE/SGP-3. Those of sLe^x-modified glycan and tyrosine sulfate TYS residues of SGP-3 are identical to our previous study (12). All simulations were performed using the program NAMD2 (26).

The CWS system included 66,390 water molecules and had dimensions of $120 \times 90 \times 60$ Å^3 ($x \times y \times z$). Before equilibration, energy minimization was done in sequence for 10,000 steps and heating to 330 K in 33-K increments every 10 ps. The system was then allowed to equilibrate freely for 200 ps in a 330-K heat bath (controlled by Langevin thermostat) and at one atm of pressure (controlled by the Nosé-Hoover Langevin piston method with a coupling coefficient of 2.0 ps^{-1}). Next, another 200-ps equilibration was manipulated by further fixing water molecules in the bottom 5 Å layer. We use the resulting equilibrated system to evaluate the proposed approach for simulating shear flow with a constant velocity gradient.

Our MCS system contained 129,823 molecules and had dimensions of $105 \times 175 \times 70$ Å^3. The original strontium ion Sr^{2+} of the crystal structure was replaced by the calcium ion Ca^{2+} because, physiologically, P-selectin/PSGL-1 interactions are Ca^{2+}-dependent (27). The physical axis of the P-LE/SGP-3 construct is defined by the vector connecting the terminal atom of the SGP-3 peptide (P618-C_α) to the terminal atom of the P-selectin epidermal-growth-factor (EGF) domain (D158-C_α). To represent the physiological orientation (Figs. 1 and 2), this axis is rotated by 60° relative to the x axis (28). We first minimized the system using 5000 steps with the fixed backbone of P-LE and of the SGP-3 peptide, the Ca^{2+} ion, and the nonhydrogen atoms of SGP-3 glycan. Further minimization was done for another 5000 steps with fixed D158-C_α and with P618-C_α constrained in the x and z directions. The system was then heated to 310 K followed by equilibration for 1 ns with the same elements of D158-C_α held fixed and P618-C_α constrained in the x and z directions, and another equilibration of 3 ns with addition of bottom 5 Å-water layer fixation. The equilibrations were performed under the same pressure, and temperature as that of the CWS system. During the second equilibration process, the root mean-square deviation (RMSD) of P-LE/SGP-3 construct with respect to the crystal structure was 1.39 ± 0.23 Å. We use this system for the subsequent dissociation simulations.

For all simulations with periodic boundary conditions, we use an integration time step of 1 fs, a uniform dielectric constant of 1.0, a cutoff of nonbonded interactions with a switching function starting at 11 Å and reaching zero at 14 Å, and a scaling factor of 1.0 for 1–4 interactions.

Shear flow field

We use the TclBC method based on the Tcl interface of the NAMD program (29) to achieve a shear flow field with constant velocity gradient. This method allows us to apply forces at each time step to water molecules in specific regions to accelerate them to the target velocity. As indicated in Fig. 1, *A* and *B*, water molecules within the bottom 5 Å layer are fixed, and those within the top 5 Å layer and the leftmost layer with thickness of 5, 10, or 15 Å are forced to move at the target velocity.

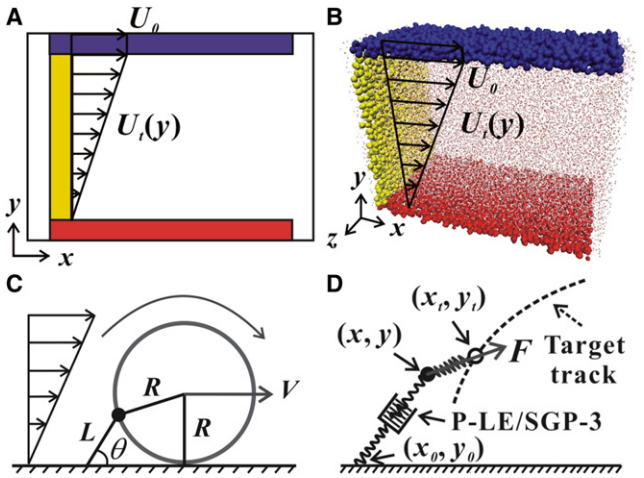

FIGURE 1 Schematic of shear flow field (*A*), CWS in NAMD (*B*), virtual-leukocyte rolling model (*C*), and TDA (*D*). (*A*) Flow field is mainly divided into four regions: bottom layer, top layer, left dragging box, and work region. Margins on both sides are set to prevent water molecules on the right side of the system from directly running into the left dragging box because of the periodic boundary condition. (*B*) Water molecules in the work region and margins at both sides are shown (*lines*), and those in other regions are displayed (denoted *VDW*). (*C*) Virtual leukocyte (*sphere*) with radius R rolls at velocity V under shear flow. The physical axis of P-LE/SGP3 is denoted (*line*) with length L connecting leukocyte and vascular surface. Angle between the line and the surface is shown (denoted as θ). (*D*) To mimic mechanical stretch on the complex (*springs in series*) from the rolling leukocyte, a virtual spring is placed between the end of the complex (*solid circle*) and its target point (*open circle*), which moves along the predefined track (*dashed line*). The dragging force F (*arrow*) points to the target point from the end of the complex.

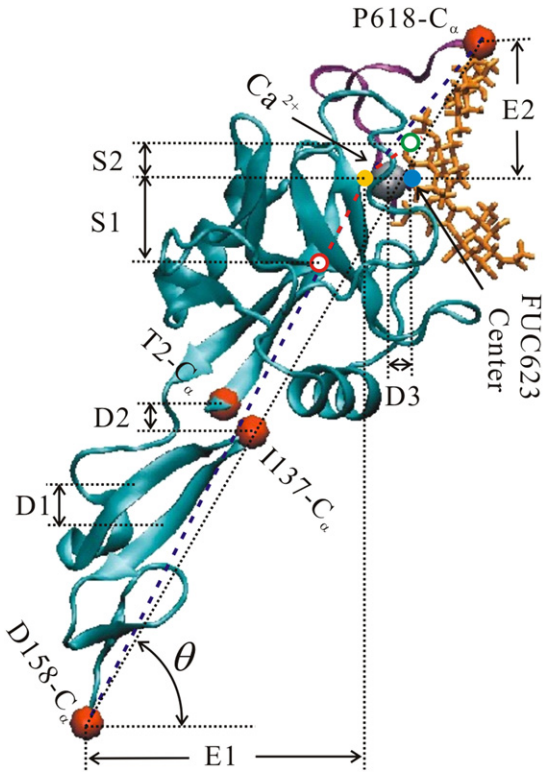

FIGURE 2 Definitions of physical parameters for structural analysis of the dissociation of the P-LE/SGP-3 construct. Extension ($E1+E2$) of the construct is the sum of the distance $E1$ between D158-C_α and the mass center of the binding sites (S46-N, S46-OG, S47-OG, N82-ND2, R85-NH1, E88-OE2, K112-N, and H114-NE2) and distance $E2$ between P618-C_α and mass center of the binding sites. Separation distance ($S1+S2$) is the sum of the distance $S1$ between the mass center of the Lec domain and the mass center of the binding sites and the distance $S2$ between the mass center of SGP-3 and the mass center of the binding sites. $D1$ represents the distance between the mass center of the backbone atoms of two key antiparallel β-sheets (G131-E135 and Y140-C144), $D2$ is the distance between T2-C_α and I137-C_α, and $D3$ is the distance between Ca^{2+} and the mass center of FUC623. The physical axis (*dotted line* linking D158-C_α and P618-C_α) of the construct makes an angle θ with the horizontal. (*Cartoon*) P-LE domains (SGP-3 ligand was shown in *ribbons* for peptide and *licorice* for glycan, respectively).

By Newton's second law, the dragging force is

$$F = M\frac{U_t(y) - U(y)}{\Delta t}, \tag{1}$$

where $U_t(y)$ is the target velocity along the x axis, $U(y)$ is the current velocity, M is the mass of the water molecule, and $\Delta t = 1$ fs is the time interval. The dragging force is applied to the oxygen atoms of the water molecules along the x axis and is recalculated at each time step. The target velocity of water molecules upon which a force is exerted is defined as

$$U_t(y) = U_0\frac{y - y_b}{y_u - y_b}, \tag{2}$$

in which U_0 is the target velocity of the whole top layer, y_b and y_u are, respectively, the minimal and maximal y coordinates of the leftmost region, and y is the instantaneous coordinate of the oxygen atom upon which the force is exerted.

We assessed the feasibility of our approach for simulating the shear flow field under three different control conditions: neither temperature- nor pressure-controlled (NTNP), temperature- but not pressure-controlled (CTNP), and both temperature- and pressure-controlled (CTCP). Because pressure control is coupled with system temperature, the case of pressure-controlled but not temperature-controlled (NTCP) is impracticable. Three velocity gradients, 1.25, 3.75, and 6.25 $\times 10^{-3}$ ps^{-1}, were selected with corresponding target velocities U_0 of 0.1, 0.3, and 0.5 Å/ps, respectively. Each simulation, with its specific control conditions, velocity gradient, and leftmost-box thickness, was repeated three times.

Track dragging approach

We developed a virtual model of a rolling leukocyte to mimic mechanical stretch and applied it to one end of a P-selectin/PSGL-1 complex (21) (Fig. 1 *C*): a virtual leukocyte of radius R rolls with velocity V, and a P-selectin/PSGL-1 complex with physical length L links the virtual cell and the vascular surface and makes an angle θ with the vascular surface. Because the length of P-LE/SGP-3 is much shorter than that of the P-selectin/PSGL-1-complex (30–32), the virtual cell shrinks by reducing the radius R_i according to

$$R_i = \frac{R_r L_1}{L_0}, \tag{3}$$

where R_r is the actual radius of the leukocyte, L_1 is the linear length of the P-LE/SGP-3 construct along the physical axis, and L_0 is the extracellular length of the P-selectin/PSGL-1 complex. We find $R_i = 0.4$ μm for $R_r = 5.0$ μm, $L_1 = 76.20$ Å, and $L_0 = 90.0$ nm. After equilibration, the angle θ of P-LE/SGP-3 varies from 60° to 65° (Fig. 1*C*).

We also modeled the tensile stretching of P-LE/SGP-3, which is caused by the rolling leukocyte, with the TclBC method (29). This stretching pulls atom P618-C_α of P-LE/SGP-3 along the predefined trajectory via a virtual spring to mimic drag on the rolling cell (Fig. 1*D*). The drag force is given as

$$F = k\left[\sum_{i=1}^{3}(x_{it} - x_i)^2\right]^{1/4}, \tag{4}$$

where the stiffness k of the virtual spring was set to 25.0 kcal/(mol·$Å^{3/2}$) or 1737 pN·$Å^{-1/2}$, in which x_i ($i = 1, 2, 3$) represents the instantaneous coordinates x, y, and z of the end of P-LE/SGP-3 that experiences the force, and x_{it} is the target coordinate, which is updated along the trajectory at each time step Δt (= 0.1 ps). We use the fourth root in Eq. 4 to get a moderate drag force to prevent excessively large or small forces. Based on the virtual model of a rolling leukocyte (Fig. 1 *C*), the coordinates of the target trajectory at time t are

$$\begin{aligned} x_t &= x_0 + Vt - R_i\sin\left(V\frac{t}{R_i} + 0.186\right) + 773.107, \\ y_t &= y_0 + R_i - R_i\cos\left(V\frac{t}{R_i} + 0.186\right), \\ z_t &= z_0, \end{aligned} \tag{5}$$

where x_0, y_0, and z_0 are the coordinates of the fixed atom D158-C_α of P-LE/SGP-3 and t is the simulation time. The rolling velocity V of the virtual leukocyte is coupled with shear flow because leukocyte rolling results from shear flow.

Both in vitro and in vivo measurements suggest that the ratio between leukocyte rolling velocity and wall shear stress (ranging from 0.085 to 0.5 Pa) is ~1.1–7.0 $\times 10^{-7}$ Å/(ps·Pa) (7,9,33). Given the ratio of 5.86 $\times 10^{-7}$ Å/(ps·Pa), we ran the TDA simulations alone or the combined TDA-SFF simulations for the MCS at a virtual-cell rolling velocity of 0.08 Å/ps, which resulted from a velocity gradient of 1.875 $\times 10^{-3}$ ps^{-1}

with a dynamic water viscosity of 8550×10^{-7} N·s/m^2, a system temperature of 300 K, and a virtual-cell radius of 0.4 μm.

Data analysis

To evaluate the quality of the constructed SFF, we calculate the velocity distribution of water molecules within different regions and their corresponding temporal evolution. A cuboid $10 \times 80 \times 20$ Å^3 in size in the central work region, 40 Å away from the left-dragging box, is divided into a series of $10 \times 10 \times 20$ Å^3 small cuboids along the y axis, and each small cuboid included ~64 water molecules. The overall velocity of each small cuboid is defined as the average velocity of the water molecules passing through it in a 20-ps time interval. To obtain sufficient data and to decrease the local computational errors, neighboring cuboids are overlapped by 5 Å along the y axis. The SFF uniformity along the x axis is similarly evaluated by calculating the overall velocities of a series of cuboids along the x axis whose geometric centers are located 45 Å above the bottom layer. We estimate the deviation of the constructed flow field from the target flow field by using the root mean-square deviation of velocities (RMSV),

$$\mathrm{RMSV} = \frac{\sqrt{\sum_{i=1}^{N}(U_i - U_t)^2}}{\sqrt{N}}, \qquad (6)$$

where U_i is the average velocity for each cuboid, U_t is the target velocity at the center of the corresponding cuboid, and N is the total number of cuboids.

The extension and separation of the molecular complex are defined to globally quantify the conformational evolution for SFF- and/or TDA-induced dissociation of the P-LE/SGP-3 construct (Fig. 2). Molecular extension includes both intermolecular dissociation and intramolecular disruption. Considering that the construct may bend under the SFF, the extension is determined by summing the two distances $E1$ and $E2$. Similarly, we determine the complex separation accompanied by intermolecular dissociation by summing the distances S1 and S2.

To further refine the intramolecular conformational changes of the P-LE domains and the intermolecular dissociation of the P-LE/SGP-3 construct, we analyze the RMSDs of backbone atoms for respective Lec (W1-A120) and EGF (S121-D158) domains relative to their own initial structures to evaluate conformational stability. We monitor the orientation change of the EGF domain relative to the Lec domain by observing the angle between two vectors: the first connects the mass center of the nonhydrogen atoms of the P-selectin-lectin/EGF interface hinge (residues A120 and S121) to that of the Lec domain (residues W1 to T119) and the second connects the same origin to the nonhydrogen atoms of the main EGF domain (residues C122 to T141).

We monitor destruction of the two main antiparallel β-sheets in the EGF domain via the distance $D1$ as well as via the corresponding hydrogen-bond number $H1$ between the two peptides. Hinge disruption between Lec and EGF domains is monitored via the distance $D2$ and the corresponding hydrogen-bond number $H2$. To characterize the dissociation of the construct, we calculate the distance $D3$ as well as the hydrogen-bond $H3$. These parameter definitions were shown in Fig. 2.

RESULTS

Feasibility of constructing shear flow field

To test the feasibility of SFF constructing, we used the CWS with a left-dragging layer thickness of 5 Å to elucidate the effect of various control parameters on the quality and stability of the shear flow. We employed three cases of temperature and pressure control and conducted corresponding MD simulations. Under CTCP conditions, the distribution of flow velocity coincided well with the target distribution after a simulation time of 40 ps with a constant gradient of 3.75×10^{-3} ps^{-1} (Fig. 3 *A*). The corresponding RMSV decreases initially and then reaches a plateau after 50 ps (Fig. 3 *D*), which suggests that a steady shear flow is obtained. This flow field remains stable during an extended 1.5-ns simulation (see Fig. S1 and Movie S1 in the Supporting Material) and is uniform along the flow direction (see Fig. S2). Moreover, under CTNP conditions, the shear flow field is also effectively constructed (Fig. 3 *B*) with a similar evolution of the RMSV (Fig. 3 *D*) and, under NTNP, the shear flow field actually fits the target flow field better (Fig. 3 *C*) with a smaller RMSV (Fig. 3 *D*).

We noticed that the shear flow under NTNP conditions is accompanied by a sharp drop in system temperature to 50 K (within 100 ps), which is far lower than the physiological temperature (see Fig. S3). In contrast, the system temperature under both CTCP and CTNP conditions remains stable near 316 K (after an initial slight reduction; see Fig. S3). This contradiction is not surprising because the temperature control is able to maintain Brownian motion of water molecules so as to reduce the motion due to the applied force, which decreases the system temperature. Taken together, CTCP conditions were eclectically adopted in the following simulations of the MCS system by considering both the physiological relevance and the numerical efficiency of the constructed shear flow field.

We also test the impact of the velocity gradient on shear flow field construction under three target gradients of 1.25, 3.75, and 6.25×10^{-3} ps^{-1} with target velocities U_0 of 0.1,

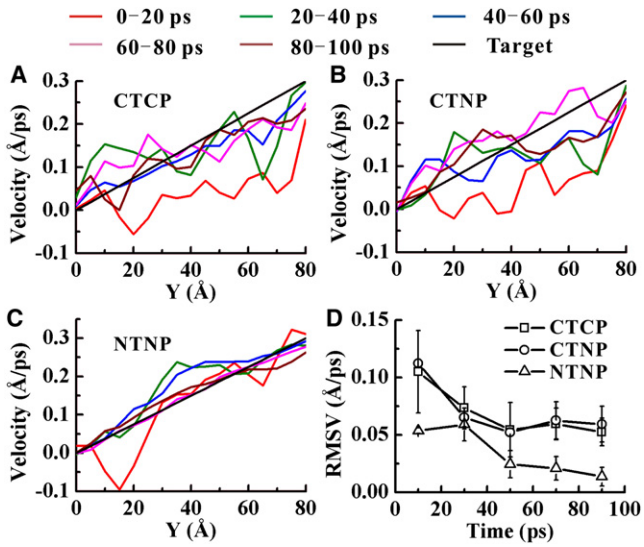

FIGURE 3 Flow velocity distribution in different time periods under various control conditions: CTCP (*A*), CTNP (*B*), and NTNP (*C*), and their RMSVs (*D*). The thickness of the left dragging box is 5 Å, and the target velocity gradient is 3.75×10^{-3} ps^{-1}. Computations were repeated in triplet and data are presented as mean ± SD in panel *D*.

0.3, and 0.5 Å/ps. The results indicate that shear flow fields are well developed under the low gradients of 1.25 and 3.75 $\times$ 10^{-3} ps^{-1} (Figs. 4 *A* and 3 *A*) and have similar RMSVs beyond 50 ps (Fig. 4 *C*) and system temperatures (see Fig. S4). At the high gradient of 6.25 $\times$ 10^{-3} ps^{-1}, however, the upper-half work region cannot reach the target velocity (Fig. 4 *B*), as indicated by the continuous increase in the RMSV after 30 ps (Fig. 4 *C*). We attribute this result to accelerated water molecules in this region being driven out so quickly that the water molecules continuously recruited into the region are too few to replace them. Thus, we use a velocity gradient of 3.75$\times$$10^{-3}$ ps^{-1} by setting the target velocity U_0 to 0.3 Å/ps in the following simulations of the MCS.

The purpose of fixing the bottom layer and uniformly driving the top layer in the SFF approach is to prevent a direct connection between the two layers due to periodic boundary conditions and to assure the quality and stability of the constructed field. With these simplifications, water molecules in the left dragging box are pushed so that their initial velocity is the target velocity and are thus effectively transmitted downstream along the x axis. We also test the effect of the thickness of the left dragging layer on the constructed shear flow. The results indicate that increasing the thickness from 5 to 10 to 15 Å does not impact the RMSV of the constructed flow field (Fig. 4 *D*) but decreases the system temperature by ~5 K (see Fig. S5). Thus, we set the thickness of the left dragging box to 5 Å in the following SFF simulations.

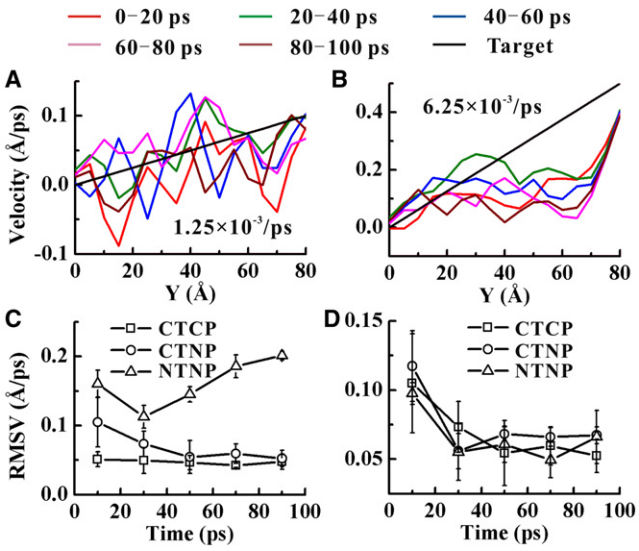

FIGURE 4 Under CTCP, flow velocity distribution at the target velocity gradient of 1.25 $\times$ 10^{-3} ps^{-1} (*A*) and 6.25 $\times$ 10^{-3} ps^{-1} (*B*), and their RMSVs over time (*C*), in which the thickness of the left dragging box is 5 Å. The dependence of the RMSVs on left-dragging-box thickness (ranging from 5 to 15 Å) is exemplified in panel *D* at the target gradient of 3.75 $\times$ 10^{-3} ps^{-1}. All the simulations were repeated in triplet and data are presented as mean $\pm$ SD in panels *C* and *D*.

We test the shear flow using the SFF approach under CTCP conditions with a 5 Å-thick top layer, a left dragging box, and a fixed bottom layer as well as a velocity gradient of 1.875 $\times$ 10^{-3} ps^{-1} with the system of MCS (see Fig. S6). Similarly, a stable shear flow field with a constant velocity gradient under CTCP conditions is effectively constructed by using an MD simulation based on the SFF approach, which provides a powerful tool to investigate the microstructural bases of dissociation of P-LE/SGP-3 construct under conditions that mimic physiological conditions.

Application of tensile stretch model

SMD, a widely used module in the NAMD program, applies two types of mechanical stretch along a fixed direction: stretch with constant velocity and stretch with constant force. However, the physiological stretch force that acts on the P-selectin/PSGL-1 complex is distinguished by momentary variations in the force direction that are caused by leukocyte rolling. We developed the TDA approach in this study to overcome the limitation of the currently available SMD module to the exertion of a force with time-varying direction and, by using Eqs. 4 and 5, to mimic the mechanical stretch that stems from cell rolling.

Upon simulating the stretching of P-LE/SGP-3 with the TDA approach, we find that the track of the end to which the force is applied is in excellent agreement with the target track for all three axes (Fig. 5), with only trivial deviations of –0.106 $\pm$ 0.115 Å (x), 0.091 $\pm$ 0.126 Å (y), and -0.002 $\pm$ 0.111 Å (z). Meanwhile, the magnitude and direction of the drag forces change with time because of the continuous change in position of the end to which the force is applied relative to the target track. The forces averaged over an entire 4.5-ns simulation are -374 $\pm$ 376 pN (x), 304 $\pm$ 404 pN (y), and -7 $\pm$ 382 pN (z). Furthermore, the TDA approach also works well when the SFF is applied to the MCS (data not shown). Thus, by using an MD simulation based on the TDA approach, we effectively model a mechanical stretch that mimics

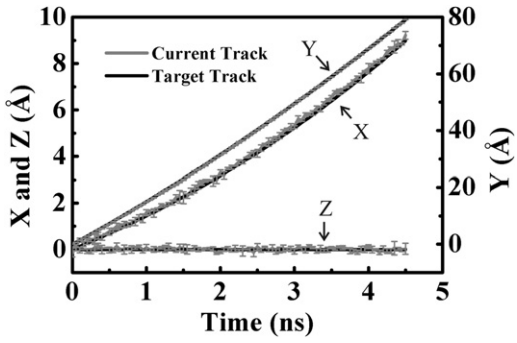

FIGURE 5 Under TDA, actual trajectories of dragged site (P618-C_α) are compared with target trajectories along all three axes. Computations were repeated in triplet and data are presented as mean $\pm$ SD.

the physiological force that results from leukocyte rolling and that acts on the P-selectin/PSGL-1 complex.

Two types of mechanical forces lead to different collapse scenarios for P-LE domains

To mimic leukocyte rolling under physiological flow, we applied a combination of the SFF and TDA approaches to the ratio of leukocyte rolling velocity to wall shear stress. We therefore further investigate the influence of the SFF and TDA approaches alone or combined on the dissociation of the P-LE/SGP-3 construct and find that the two types of mechanical forces induce the dissociation of P-LE/SGP-3 in different ways.

First, we observe a distinct structural collapse when the P-LE/SGP-3 construct is subjected to an SFF and/or track dragging (see Movie S2, Movie S3, and Movie S4). For example, as seen in Fig. 6 *A*, the construct extension increases linearly at the rate of 0.086, 0.072, and 0.016 Å/ps for TDA+SFF, SFF, and TDA, respectively—all of which results in remarkable conformational changes. Complex separation exhibits a steady phase initially (when the separation distance remains unchanged), followed by a transition phase during which the separation distance increases linearly with extension distance. Thus, construct dissociation does not occur when the extension is less than the threshold extension (*arrows* in Fig. 6 *B*), which suggests that intramolecular collapse happens before construct dissociation. Combined with the transition threshold values (estimated from the separation-extension curve shown in Fig. 6 *B*) of 30, 50, and 23 Å for TDA+SFF, SFF, and TDA, respectively, these results indicate that SFF and TDA have different impacts on the structural disruption of the P-LE/SGP-3 construct; that is, before construct dissociation, SFF induces a more remarkable intramolecular collapse than TDA.

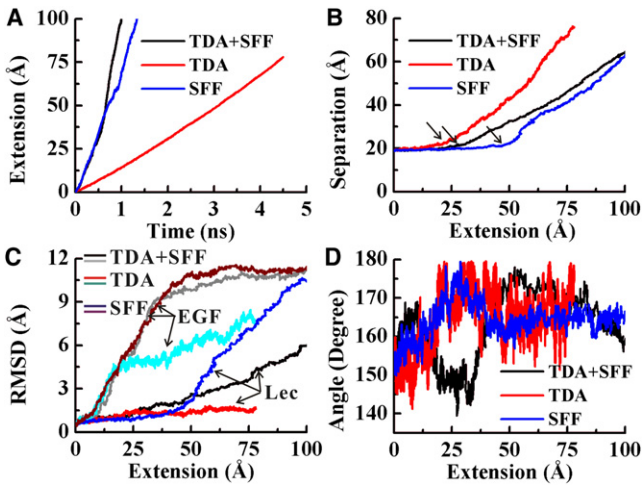

FIGURE 6 Under three mechanical stimuli, evolutions of construct extension (*A*), dependence on construct extension of the separation distance (*B*), RMSD of the EGF and Lec domains against their initial structures (*C*), and hinge angle between the Lec and EGF domains (*D*).

Second, we analyze the structural bases of different intramolecular collapse scenarios of the P-LE receptor. The evolution of the RMSDs of the Lec and EGF domains indicates that the EGF domain is destroyed at an early stage (a transition threshold of ~5 Å) under TDA+SFF, SFF, and TDA, whereas a more severe disruption is found with larger RMSDs (~11 Å) under TDA+SFF and SFF than the disruption with an RMSD of ~8 Å under TDA at the equilibrium stage (Fig. 6 *C*). By contrast, the Lec domain tends to retain its conformation with small and stable RMSDs (Fig. 6 *C*) even though its conformation is enhanced after construct dissociation under TDA+SFF and SFF (Fig. 6 *C*). This effect is further confirmed by hinge breakage between the Lec and EGF domains. Under three types of mechanical stimuli, we find similar increases in the angle between the Lec and EGF domains (from an initial value of ~150° to a higher value of 165° to 175°), with the evolution in angle spanning the duration of construct dissociation (Fig. 6 *D*). We tentatively attribute the descending phases before and after dissociation under TDA+SFF to the rotation and additional destruction of the Lec domain (Fig. 6 *D*). Together, these results indicate that the P-LE collapse mainly concerns the EGF domain and the hinge region between the Lec and EGF domains.

Third, we further test the conformational change within the EGF domain, especially in regard to its main components of two antiparallel β-sheets (G131-E135 and Y140-C144). Consistent with the evolution in the RMSD of the EGF domain, the distance between the two β-sheets ($D1$) initially remains constant then increases starting from an extension of ~20 Å (TDA+SFF and SFF) and of ~30 Å (TDA), before finally reaching a high plateau of ~21 Å and low plateau of ~9 Å, respectively (Fig. 7 *A*). Accordingly, the number of hydrogen bonds between the two β-sheets (H1) first decreases then becomes stable, concurrent with the transition in $D1$ (Fig. 7 *B*). The high RMSD in the EGF domain of ~10 Å (Fig. 6 *C*) and the large distance $D1$ of ~20 Å between the two β-sheets (Fig. 7 *A*) under TDA+SFF and SFF show a similar trend; namely, that SFF induces a more thorough intramolecular collapse than TDA alone.

We see the hinge opening given by the distance $D2$ between T2-C_α and I137-C_α increases slowly at first and then reaches a plateau at ~30 Å under TDA+SFF and SFF and at ~20 Å under TDA (Fig. 7 *C*). Again, the number of hydrogen bonds between the Lec and EGF domains (H2) decreases rapidly to zero under TDA+SFF and SFF, whereas it remains occasionally nonzero under TDA (Fig. 7 *D*). Together, the forced dissociation of the P-LE/SGP-3 construct occurs after the intramolecular disruption of P-LE, which focuses on the EGF domain and the interface hinge between the EGF and Lec domains. The differences in the P-LE collapse scenario between TDA+SFF

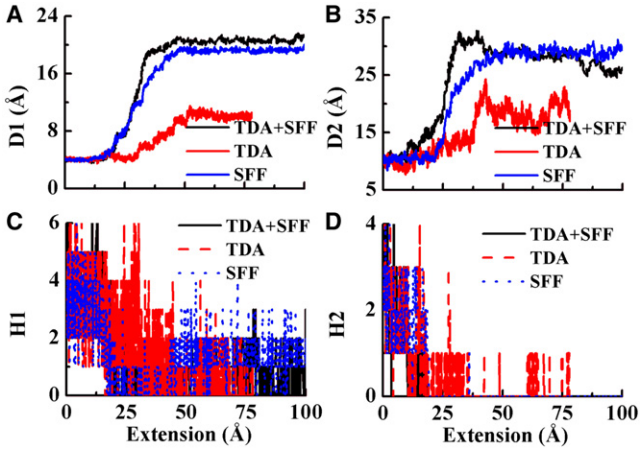

FIGURE 7 Under three mechanical stimuli, dependence on construct extension of the distance between the mass center of backbone atoms of two antiparallel β-sheets (G131-E135 and Y140-C144) (*A*), of the number of hydrogen bonds between the two β-sheets (*B*), of the distance between T2-C_α and I137-C_α (*C*), and of the number of hydrogen bonds within the hinge region between the Lec and EGF domains (*D*).

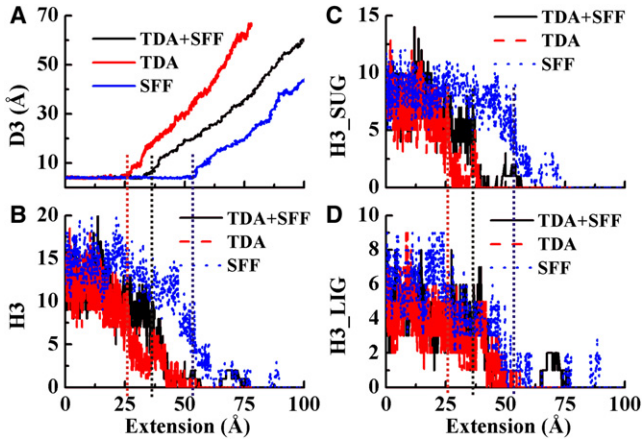

FIGURE 8 Under three mechanical stimuli, dependence on construct extension of the distance between Ca^{2+} and the mass center of FUC623 (*A*), of the number of hydrogen bonds in P-LE-SGP3 interface (*B*), of the number of hydrogen bonds between P-LE and SUG (*C*), and of the number of hydrogen bonds between P-LE and LIG (*D*).

or SFF and TDA highlights the distinct roles of SFF and TDA in P-LE conformational changes.

Two types of mechanical forces induce similar dissociation scenario of P-LE/SGP-3 construct

In contrast to the intramolecular collapse, the intermolecular dissociation of the P-LE/SGP-3 construct under TDA+SFF, SFF, and TDA presents similar features. For example, the distance *D*3 between the Ca^{2+} ion and the mass center of the sugar residue FUC623 increases linearly after an initial steady phase (Fig. 8 *A*), and the transition thresholds precisely correspond to those from the separation-extension profile (Fig. 6 *B*). This result implies that the interaction between Ca^{2+} and FUC623 is the key interaction of the binding interface and that their separation is the primary indicator of dissociation of the P-LE/SGP-3 construct.

This conclusion is also supported by the sharp reduction in the corresponding number H3 of hydrogen bonds that starts at different time delays for the different simulation scenarios (Fig. 8, *A* and *B*). Moreover, the separation of all sugar residues of the SGP-3 ligand from the P-LE receptor is represented by the number H3_SUG of hydrogen bonds, which is consistent with that of the Ca^{2+}-FUC623 interaction (Fig. 8 *C*). In addition, the peptide residues of the SGP-3 ligand dissociate from P-LE with a slight delay, as seen in the evolution of the H3_LIG hydrogen bonds (Fig. 8 *D*).

In summary, our MD simulations of dissociation of the P-LE/SGP-3 construct under TDA+SFF, SFF, or TDA indicate that intramolecular collapse of P-LE happens before construct dissociation, which mainly focuses on the two major antiparallel β-sheets of the EGF domain and the hinge interface between the EGF and Lec domains. We attribute the intermolecular disruption of the P-LE-SGP-3 construct mainly to the separation of Ca^{2+} from FUC623. These features are similar to those found in our SMD simulations in previous work (12). Our results also indicate that the SFF and TDA approaches have different impacts on P-LE/SGP-3 interactions in intramolecular collapse but not on interface disruption. Conformational analysis of the P-LE extension, the complex separation, as well as the collapse of the EGF domain and the P-selectin-lectin/EGF hinge imply that the impact of shear flow cannot be neglected in MD simulations of complex dissociation. When using the physiological ratio of leukocyte rolling velocity/wall shear stress, our simulations indicate that, before complex dissociation, shear flow induces more intermolecular destruction than does tensile stretch.

DISCUSSION

The P-selectin/PSGL-1 complex is subjected to mechanical stretching from the rolling leukocyte and to shear stress from blood flow, and the modulation of these two types of mechanical forces on the dissociation kinetics of the P-selectin/PSGL-1 complex is crucial to the corresponding physiological functions. The currently existing limitations of experimental assays and simulation approaches have thus far prevented researchers from isolating the impact of shear stress and from clarifying the influence of an external force with time-varying direction and magnitude. In this study, we developed two approaches, SFF and TDA, to mimic the mechanical loading of the physiological microenvironment using MD simulations (Fig. 1). The microscopic structural bases of the P-LE/SGP-3 construct under SFF and/or TDA are analyzed using a virtual rolling-leukocyte model.

In our estimation, the novelty of this study lies in the following two aspects:

The first is that it extends the current MD simulation approaches. In a sufficiently long simulation, the SFF approach developed in this work mimics shear flow with a linear velocity distribution. Compared with the previously described "uniform" flow fields with constant velocity (16–18), our approach successfully mimics the shear stress of blood flow in the boundary layer near the venular surface, at least in a velocity-gradient range of 1.25 to 3.75×10^{-3} ps^{-1} (Figs. 3 and 4). The TDA approach developed herein successfully implements a tensile stretch that has a time-varying direction and magnitude and follows a preset trajectory. This approach mimics the mechanical stretch exerted on the P-selectin/PSGL complex by the rolling leukocyte. Numerically, our approach overcomes the limitation of loading constant velocity or constant force along a fixed direction in SMD (Fig. 5). Note that the virtual rolling-leukocyte model is based on the hypothesis that the leukocyte is an ideal sphere and rolls purely at constant velocity. Further studies are required to optimize the rolling-leukocyte model by integrating the jump model observed in vitro (6) and to investigate the impacts of leukocyte inhomogeneity and deformability. Lees-Edwards boundary condition approach is widely used to generate linear shear flow (34,35) with a underlying assumption that the flow distribution will not be disturbed by the existence of target particle. But it will produce an unreal shear flow field locally around the studied macromolecule. The SFF approach established here is applicable for studying the microscopic behaviors of protein molecule in a scale of Ångstroms and evaluating the interactions of each water molecule and target protein.

The second novel (to our knowledge) aspect of our study is that it illustrates the remarkable impact of shear flow on P-LE/SGP-3 dissociation. Although the conformational evolution of the P-LE/SGP-3 construct under each type of mechanical stimulus (Figs. 6–8) is similar to that obtained with the previously described SMD simulations (12), the simulations presented here also indicate that shear stress more strongly impacts P-LE/SGP-3 dissociation than does point-directed mechanical stretch. The relative contribution of these two forces is revealed mainly by the degree of intramolecular collapse of P-LE before construct dissociation, and SFF or TDA+SFF induces more significant P-LE collapse than does TDA. These simulations explicate the modulation of physiology-mimicking shear flow on P-selectin/PSGL-1 interactions and offer clues to the role of isolated shear stress on receptor-ligand interactions. They indicate not only that the shear stress is functional for the transportation of molecular carriers along the flow, but also that it works effectively as a mechanical modulator of the dissociation of the molecular complex.

It is undeniable that some simplifications exist in our models. For example, we considered the leukocyte to be a rigid sphere, took the P-selectin/PSGL-1 complex to be a linear spring, and transformed the virtual leukocyte in proportion to the length ratio between the P-LE/SGP-3 construct and the P-selectin/PSGL-1 complex (the latter was to ensure that the extension of P-LE/SGP-3 construct coincided with the velocity of the rolling leukocyte). In addition, some parameters used in this study are beyond the physiological ranges. For instance, the velocity gradient and virtual-leukocyte rolling velocity were approximately six orders-of-magnitude higher than measured, although the track dragging force (average ~800 pN in this study) was the same order of magnitude as is found experimentally (~104 pN (36) or ~155 pN (37)). However, it is the rolling velocity of virtual cell (i.e., elongation rate and extent of protein complex) that determines its conformational disruption, and not the track dragging force itself; the latter is just to constrain the forced complex-end to the predefined rolling trajectory and keep the trajectory consistent between dragging point and rolling cell. Therefore the controlling parameters in SFF and TDA, i.e., the velocity gradient and elongation rate, were comparable.

Regardless of the inevitable limitations on computational capacity, our simulations offer valuable information for exploring the structure-function relationship of single molecules or molecular complexes of interest (13,16–18). Thus, this study provides two useful concepts in that it mimics the physiological shear stress and the mechanical stretch with varying direction and magnitude, and it offers clues for better understanding the physiological role of shear stress on the interactions involved in the dissociation of P-selectin/PSGL-1 as well as other receptor-ligand interactions.

SUPPORTING MATERIAL

Six figures and four movies are available at http://www.biophysj.org/biophysj/supplemental/S0006-3495(11)05353-7.

MD simulations were performed at the Supercomputing Center, Chinese Academy of Sciences and on the Computing Facility for Computational Mechanics, Institute of Mechanics, Chinese Academy of Sciences.

This work was supported by the National Natural Science Foundation of China (30970707, 10702075, and 30730032), the National High-Technology Research and Development Program of China 2009AA02Z407), the National Key Basic Research Foundation of China (2011CB710904), and the Knowledge Innovation Project of the Chinese Academy of Sciences (KJCX2-YW-L08).

REFERENCES

1. McEver, R. P., J. H. Beckstead, …, D. F. Bainton. 1989. GMP-140, a platelet α-granule membrane protein, is also synthesized by vascular endothelial cells and is localized in Weibel-Palade bodies. *J. Clin. Invest.* 84:92–99.

2. Moore, K. L., N. L. Stults, …, R. P. McEver. 1992. Identification of a specific glycoprotein ligand for P-selectin (CD62) on myeloid cells. *J. Cell Biol.* 118:445–456.

3. McEver, R. P., K. L. Moore, and R. D. Cummings. 1995. Leukocyte trafficking mediated by selectin-carbohydrate interactions. *J. Biol. Chem.* 270:11025–11028.
4. Moore, K. L., K. D. Patel, …, R. P. McEver. 1995. P-selectin glycoprotein ligand-1 mediates rolling of human neutrophils on P-selectin. *J. Cell Biol.* 128:661–671.
5. Alon, R., D. A. Hammer, and T. A. Springer. 1995. Lifetime of the P-selectin-carbohydrate bond and its response to tensile force in hydrodynamic flow. *Nature.* 374:539–542.
6. Zhu, C., T. Yago, …, R. P. McEver. 2008. Mechanisms for flow-enhanced cell adhesion. *Ann. Biomed. Eng.* 36:604–621.
7. Atherton, A., and G. V. R. Born. 1973. Relationship between the velocity of rolling granulocytes and that of the blood flow in venules. *J. Physiol.* 233:157–165.
8. Marshall, B. T., M. Long, …, C. Zhu. 2003. Direct observation of catch bonds involving cell-adhesion molecules. *Nature.* 423:190–193.
9. Chen, S. Q., and T. A. Springer. 1999. An automatic braking system that stabilizes leukocyte rolling by an increase in selectin bond number with shear. *J. Cell Biol.* 144:185–200.
10. Evans, E., A. Leung, …, C. Zhu. 2004. Mechanical switching and coupling between two dissociation pathways in a P-selectin adhesion bond. *Proc. Natl. Acad. Sci. USA.* 101:11281–11286.
11. Lü, S. Q., and M. Long. 2004. Forced extension of P-selectin construct using steered molecular dynamics. *Chin. Sci. Bull.* 49:10–17.
12. Lü, S. Q., and M. Long. 2005. Forced dissociation of selectin-ligand complexes using steered molecular dynamics simulation. *Mol. Cell. Biomech.* 2:161–177.
13. Lou, J. Z., and C. Zhu. 2007. A structure-based sliding-rebinding mechanism for catch bonds. *Biophys. J.* 92:1471–1485.
14. Yago, T., A. Leppänen, …, R. P. McEver. 2002. Distinct molecular and cellular contributions to stabilizing selectin-mediated rolling under flow. *J. Cell Biol.* 158:787–799.
15. Schmidtke, D. W., and S. L. Diamond. 2000. Direct observation of membrane tethers formed during neutrophil attachment to platelets or P-selectin under physiological flow. *J. Cell Biol.* 149:719–730.
16. Chen, Z. Z., J. H. Lou, …, K. Schulten. 2008. Flow-induced structural transition in the β-switch region of glycoprotein Ib. *Biophys. J.* 95:1303–1313.
17. Lou, J. Z., and C. Zhu. 2008. Flow induces loop-to-β-hairpin transition on the β-switch of platelet glycoprotein Ibα. *Proc. Natl. Acad. Sci. USA.* 105:13847–13852.
18. Zou, X. Q., Y. X. Liu, …, K. Schulten. 2010. Flow-induced β-hairpin folding of the glycoprotein Ibα β-switch. *Biophys. J.* 99:1182–1191.
19. Gratton, Y., and G. W. Slater. 2005. Molecular dynamics study of tethered polymers in shear flow. *Eur Phys J E Soft Matter.* 17:455–465.
20. Delgado-Buscalioni, R., and P. V. Coveney. 2006. Structure of a tethered polymer under flow using molecular dynamics and hybrid molecular-continuum simulations. *Physica A.* 362:30–35.
21. Somers, W. S., J. Tang, …, R. T. Camphausen. 2000. Insights into the molecular basis of leukocyte tethering and rolling revealed by structures of P- and E-selectin bound to SLe(X) and PSGL-1. *Cell.* 103:467–479.
22. Humphrey, W., A. Dalke, and K. Schulten. 1996. VMD: visual molecular dynamics. *J. Mol. Graph.* 14:33–38, 27–28.
23. Jorgensen, W. L., J. Chandrasekhar, …, M. L. Klein. 1983. Comparison of simple potential functions for simulating liquid water. *J. Chem. Phys.* 79:926–935.
24. MacKerell, A. D., D. Bashford, …, M. Karplus. 1998. All-atom empirical potential for molecular modeling and dynamics studies of proteins. *J. Phys. Chem. B.* 102:3586–3616.
25. Foloppe, N., and A. D. MacKerell. 2000. All-atom empirical force field for nucleic acids: I. Parameter optimization based on small molecule and condensed phase macromolecular target data. *J. Comput. Chem.* 21:86–104.
26. Kale, L., R. Skeel, …, K. Schulten. 1999. NAMD2: greater scalability for parallel molecular dynamics. *J. Comput. Phys.* 151:283–312.
27. Geng, J. G., G. A. Heavner, and R. P. McEver. 1992. Lectin domain peptides from selectins interact with both cell surface ligands and Ca^{2+} ions. *J. Biol. Chem.* 267:19846–19853.
28. Shao, J. Y., H. P. Ting-Beall, and R. M. Hochmuth. 1998. Static and dynamic lengths of neutrophil microvilli. *Proc. Natl. Acad. Sci. USA.* 95:6797–6802.
29. Phillips, J. C., R. Braun, …, K. Schulten. 2005. Scalable molecular dynamics with NAMD. *J. Comput. Chem.* 26:1781–1802.
30. Ushiyama, S., T. M. Laue, …, R. P. McEver. 1993. Structural and functional characterization of monomeric soluble P-selectin and comparison with membrane P-selectin. *J. Biol. Chem.* 268:15229–15237.
31. Johnston, G. I., R. G. Cook, and R. P. McEver. 1989. Cloning of GMP-140, a granule membrane protein of platelets and endothelium: sequence similarity to proteins involved in cell adhesion and inflammation. *Cell.* 56:1033–1044.
32. Li, F. G., H. P. Erickson, …, R. P. McEver. 1996. Visualization of P-selectin glycoprotein ligand-1 as a highly extended molecule and mapping of protein epitopes for monoclonal antibodies. *J. Biol. Chem.* 271:6342–6348.
33. Jones, D. A., O. Abbassi, …, C. W. Smith. 1993. P-selectin mediates neutrophil rolling on histamine-stimulated endothelial cells. *Biophys. J.* 65:1560–1569.
34. Lees, A. W., and S. F. Edwards. 1972. Computer study of transport processes under extreme conditions. *J. Phys. C Solid State Phys.* 5:1921–1928.
35. Kobayashi, H., and R. Yamamoto. 2011. Implementation of Lees-Edwards periodic boundary conditions for direct numerical simulations of particle dispersions under shear flow. *J. Chem. Phys.* 134:064110.
36. Evans, E. A., and D. A. Calderwood. 2007. Forces and bond dynamics in cell adhesion. *Science.* 316:1148–1153.
37. McEver, R. P., and C. Zhu. 2010. Rolling cell adhesion. *Annu. Rev. Cell Dev. Biol.* 26:363–396.